scientific reports

Check for updates

OPEN

Modeling the CO_2 separation capability of poly(4-methyl-1-pentane) membrane modified with different nanoparticles by artificial neural networks

Seyyed Amirreza Abdollahi✉ & Seyyed Faramarz Ranjbar

Membranes are a potential technology to reduce energy consumption as well as environmental challenges considering the separation processes. A new class of this technology, namely mixed matrix membrane (MMM) can be fabricated by dispersing solid substances in a polymeric medium. In this way, the poly(4-methyl-1-pentene)-based MMMs have attracted great attention to capturing carbon dioxide (CO_2), which is an environmental pollutant with a greenhouse effect. The CO_2 permeability in different MMMs constituted of poly(4-methyl-1-pentene) (PMP) and nanoparticles was comprehensively analyzed from the experimental point of view. In addition, a straightforward mathematical model is necessary to compute the CO_2 permeability before constructing the related PMP-based separation process. Hence, the current study employs multilayer perceptron artificial neural networks (MLP-ANN) to relate the CO_2 permeability in PMP/nanoparticle MMMs to the membrane composition (additive type and dose) and pressure. Accordingly, the effect of these independent variables on CO_2 permeability in PMP-based membranes is explored using multiple linear regression analysis. It was figured out that the CO_2 permeability has a direct relationship with all independent variables, while the nanoparticle dose is the strongest one. The MLP-ANN structural features have efficiently demonstrated an appealing potential to achieve the highest accurate prediction for CO_2 permeability. A two-layer MLP-ANN with the 3-8-1 topology trained by the Bayesian regulation algorithm is identified as the best model for the considered problem. This model simulates 112 experimentally measured CO_2 permeability in PMP/ZnO, PMP/Al_2O_3, PMP/TiO_2, and PMP/TiO_2-NT with an excellent absolute average relative deviation (AARD) of lower than 5.5%, mean absolute error (MAE) of 6.87 and correlation coefficient (R) of higher than 0.99470. It was found that the mixed matrix membrane constituted of PMP and TiO_2-NT (functionalized nanotube with titanium dioxide) is the best medium for CO_2 separation.

Recently, the capture and sequestration of CO_2 (carbon dioxide)[1,2] as a practical tool against global warming and climate change have received significant interest. According to the literature, the CO_2 concentration in the atmosphere since the pre-industrial era till now has dramatically increased from 280 to 420 ppm, while its maximum allowable value is 350 ppm[3,4]. On the other hand, it has been estimated that the CO_2 concentration in the atmosphere will reach 570 ppm by the current rising level at the end of 21 century[5]. On this ground, several agreements are established to reduce CO_2 emissions by 2050 by focusing on deploying carbon capture and storage (CCS) strategies[6]. To this end, different technologies, such as absorption[7], adsorption[8,9], cryogenic[10], and membranes[11] have been proposed. However, absorption as the most mature technology owns some serious drawbacks, including corrosion of equipment[12], environmental side-effects[13], and cost[14]. Cryogenic as another mature technology consumes high energy[15]. Moreover, introducing a water-stable adsorbent with high selectivity and loading capacity as well as proper heat of adsorption and reasonable cost for the large-scale application is

Faculty of Mechanical Engineering, University of Tabriz, Tabriz, Iran. ✉email: s.a_abdollahi@yahoo.com

still a serious challenge[7,16,17]. Hence, membrane technology regarding being environmentally friendly, efficient, flexible, cost, maturity, and simple is considered one of the interesting strategies for gas separation[18] and pollution monitoring[19]. CO_2 capture and sequestration not only is crucial for post-combustion applications related to flue gas for CO_2/N_2 separation but also is required for pre-combustion processes for developing renewable sources of energy, including biogas upgrading[20] and natural gas sweetening for CO_2/CH_4 separation[21]. The recovered carbon dioxide is also possible to use as feedstock to synthesize value-added chemicals[22].

Routinely, membranes are developed in natural or synthetic ways[23], and the last one is categorized as organic and inorganic[24]. To improve the gas separation performance of conventional membranes the focus is concentrated on polymeric media[25]. To this end, different polymers, including siloxanes[26], poly acetylenes[27], polyimides[28], polysulfone[29], and basic silicon polymers[30] are employed for different separation purposes. However, polymeric membranes still have some concerns related to their permeability[31], selectivity[32], and stability at high pressures[33]. Accordingly, nanocomposite membranes are fabricated by adding starch[34], ceramic[35], metal–organic framework[36], carbon nanotube[37], and nanoparticle[38–40], to the membrane body.

On these grounds, Ahn et al. added silica nano samples as fillers to the polysulfone membrane to boost the performance of the developed mixed matrix membrane[41]. They reported inclusion of nano silica samples into the polymer structure improves the permeability. Also, Pechaf et al. applied polyimide membrane and zeolite as the MMM and assessed the permeability of He, CH_4, CO_2, N_2, and O_2[42]. They claimed the fabricated membrane increases the permeability of CO_2 and CH_4, while some reduction was observed for N_2 and O_2 permeability. Further, Ismail et al. synthesized a mixed matrix membrane using poly-ether-sulfone and Matrimid 5218 by employing Zeolite 4A[43]. The study showed adding the zeolite can improve the permeability of the membrane.

Recently, machine learning (ML) models due to their flexibility, robustness, precision, and adaptability have received significant interest in a broad range of applications from engineering to medicine[44–47]. Pattern design, model recognition, fault detection, data mining, and function estimation are some of the main applications of ML[48,49]. Recently, artificial neural network (ANN)[50], adaptive neuro-fuzzy inference system (ANFIS)[51], support vector machine (SVM)[52], and genetic programming (GP)[53] have been used in the field of membrane technology. On these grounds, Rezakazemi et al. employed the ANFIS model for molecular separation in microporous membranes[54]. In another study, Vural et al. employed ANFIS topology for estimating the performance of a proton exchange membrane fuel cell[55]. In addition, Zhao et al. employed the ANN paradigm to predict the interfacial interactions and fouling in a membrane bioreactor[56]. They declared that the radial basis function has excellent ability to predict interfacial interactions. Further, Gasós et al. trusted on the artificial neural networks to create the maps of membrane-based CO_2 separation technology[18]. Additionally, Kazemian et al. employed the benefits of SVM and genetic algorithm (GA) methodology to develop an algorithm for the membrane helices in amino acid sequences[57].

Despite conducting many experiments on measuring CO_2 permeability in pure poly(4-methyl-1-pentane) (PMP) and PMP-containing mixed membranes, no correlation has already been suggested in this field. Since permeability is a crucial factor in efficient CO_2 separation by the PMP-based membranes, a reliable model is also required for its estimation. Hence, this study applies the MLP-ANN to correlate CO_2 permeability in pure PMP and PMP/nanoparticle mixed matrix membranes to the filler type, nanoparticle dose, and pressure. Also, the performed relevancy analysis by the MLR (i.e., multiple linear regression) clarifies the effect of these variables on the potential level of CO_2 permeability. To the best of the authors' knowledge, this is the first attempt to predict CO_2 permeability in PMP-containing membranes from some easily and always available parameters. Also, the designed MLP-ANN can help engineers fabricate a PMP-based membrane and adjust the working pressure to achieve maximum CO_2 separation in various industries including gas processing, petroleum, petrochemical, as well as biogas upgrading.

Gathered data from the literature

As already discussed, permeability is one of the key specifications of membrane technology for gas separation, which is often experimentally measured. On the other hand, several other studies have investigated the impact of employing different nanoparticles to improve the performance of polymetric membranes to this end. Accordingly, this study has developed a robust theoretical topology to estimate the CO_2 permeability in the pure PMP and PMP/nanoparticle mixed matrix membranes, which to the best of the authors' knowledge is the first one in this area. In this way, the nanoparticle types, their weight percentage (wt%) in the fabricated membrane, and operating pressure are the independent variables to estimate the CO_2 permeability in a specific membrane. Table 1 presents the main statistical features of the gathered experimental data from the literature[58–61].

It is noteworthy that the literature has added up to 40 wt% of four nanoparticles (i.e., TiO_2, ZnO, Al_2O_3, and TiO_2-NT) to the PMP structure to fabricate different mixed matrix membranes. Also, 112 CO_2 permeability tests have been conducted in a pressure range of 2–25 bar. The CO_2 permeability of 18.01-570.90 barrer was

Variable	Minimum	Maximum	Average	Std. deviation	Tests
Additive type	Nothing, ZnO, Al_2O_3, TiO_2, and TiO_2-NT				112
Nanoparticle dose (wt%)	0	40	10.11	9.96	112
Pressure (bar)	2	25	5.86	3.49	112
CO_2 permeability (barrer)	18.01	570.90	199.36	120.57	112

Table 1. Literature data for the CO_2 separation by the PMP-nanoparticle membranes[58–61].

reported in the literature for the pure PMP and PMP/ZnO, PMP/Al_2O_3, PMP/TiO_2, and PMP/TiO_2-NT mixed matrix membranes[58–61].

Since this study includes both qualitative (additive type) and quantitative (nanoparticle dose and pressure) independent variables, it is also necessary to represent the earlier quantitatively. Table 2 introduces the numerical codes used in this regard.

Histograms of all independent (additive type, nanoparticle dose, and pressure) and dependent (CO_2 permeability) variables are depicted in Fig. 1.

Artificial neural networks

Artificial neural networks (ANNs) as a biologically inspired computational approach is a non-linear topology, which has a high capacity for data processing in the engineering area[62]. Actually, the ANNs are a reduced set of concepts derived from biological neural systems based on the simulation of data processing of the human brain and nervous systems[63]. The ANNs have already proved a robust potential for statistical analysis in the area without a broad range of experimental values regarding their flexibility and capability[62,63]. In the way of deriving an ANN paradigm, it is required to specify the main independent variables that affect the output of the process. It is worth noting that the ANNs have the potential to correlate the dependent variables with the independent ones with any degree of complexity[64]. To this end, providing a proper dataset is necessary to design a black box for the estimation of dependent factors considering defined criteria[62]. Accordingly, the obtained approach develops a signal among the input and output factors, which specifies the details in different layers related to neuron interactions.

Up to date, several ANN approaches have been developed, including multi-layer perceptron (MLP-ANN)[65], radial basis function (RBF-ANN)[66], cascade feedforward (CFF-ANN)[67], general regression (GR-ANN)[68], which the MLP-ANN is the most commonly used one. Generally, the MLP-ANN is an online learning supervised procedure that employs partial fit order together with tunable synaptic weights[69]. On these grounds, this topology was applied in this work to estimate the permeability of CH_4 and N_2 in PMPs. Routinely, an MLP-ANN is developed by defining three main layers, including the input layer, the hidden layer, and the output one. In this way, the input layer is derived from the raw independent (input) values after some data processing, which has

Additive name	Nothing	ZnO	TiO_2	TiO_2-NT	Al_2O_3
Additive code	0	1	2	3	4

Table 2. The numerical codes used to quantitatively presentation of the filler type.

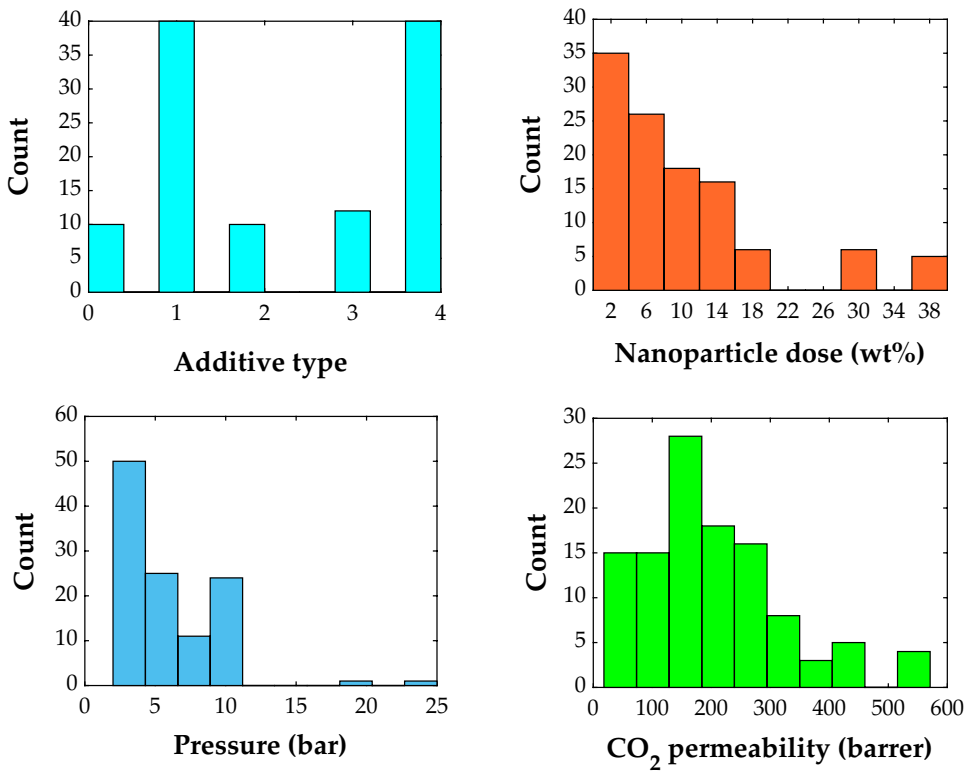

Figure 1. Histogram of the involved variables (additive type, nanoparticle dose, and pressure) in the modeling of CO_2 permeability in PMP-nanoparticle membranes[58–61].

already proven their high impact on the process. Then, the outcome of this layer is introduced to the hidden layer to employ statistical analysis and mathematical treatment on the data. Afterward, the outcomes of this layer are transferred to the output layer that specifies the main results of the model. It should be considered that the major mathematical processing employed on the neurons is determined by Eq. (1)[70]:

$$O_j = \sum_{r=1}^{N} w_{jr} x_r + b_j \tag{1}$$

here b specifies the bias of the model, which indicates the activation thresholds for input values (x_r), and ω_{jr} is the weight coefficients of the model. Also, the net output of neurons (O_j) is received by a transfer function (tf) to calculate the neuron's output[70]. In this work, the hyperbolic tangent sigmoid (Eq. 2) and logarithmic sigmoid (Eq. 3), which are among the most popular transfer functions, have been incorporated in the hidden and output layers, respectively[63,68]:

$$tf\left(O_j\right) = \frac{e^{O_j} - e^{-O_j}}{e^{O_j} + e^{-O_j}} \tag{2}$$

$$tf\left(O_j\right) = \frac{1}{1 + e^{-O_j}} \tag{3}$$

Figure 2a,b show the general shapes of the hyperbolic tangent sigmoid and logarithmic sigmoid transfer functions, respectively. This figure indicates that the earlier provides a value between − 1 and + 1, while the latter produces a value ranging from 0 to + 1.

To this end, it is necessary to normalize both the independent (IV) and dependent variables (DV) into the [0 1] range using Eqs. (4) and (5), respectively.

$$X_i^j = \left(IV_i^j - \min\left(IV_i\right)\right)/\left(\max\left(IV_i\right) - \min\left(IV_i\right)\right) \begin{cases} i = 1, 2, 3 \\ j = 1, 2, ..., NoD \end{cases} \tag{4}$$

$$Y^j = \left(DV^j - \min\left(DV\right)\right)/\left(\max\left(DV\right) - \min\left(DV_i\right)\right) \quad j = 1, 2, ..., NoD \tag{5}$$

NoD designates the number of datasets. X_1, X_2, and X_3 indicate the normalized value of the additive type, nanoparticle dose, and pressure. Moreover, Y stands for the normalized CO_2 permeability.

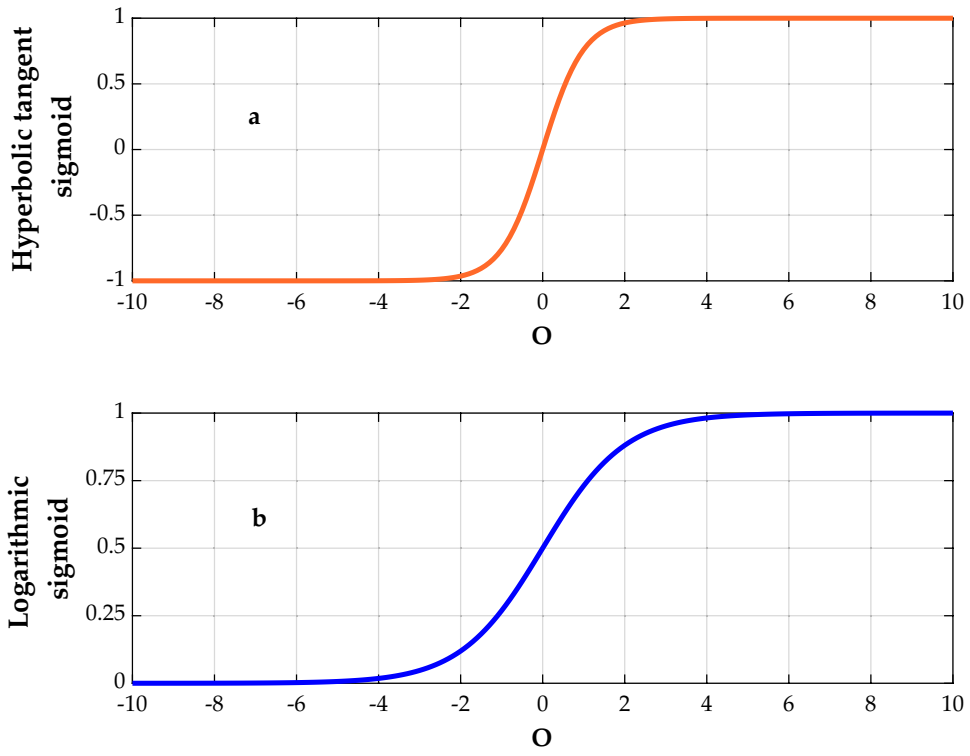

Figure 2. The hyperbolic tangent sigmoid (**a**) and logarithm sigmoid (**b**) transfer functions.

Evaluation of the model's accuracy

It is often mandatory to measure the deviation between experimental and predicted values of the dependent variable using statistical criteria. This study applies correlation coefficient (R), coefficient of determination (R^2), summation of absolute error (SAE), mean absolute error (MAE), absolute average relative deviation (AARD), and mean squared error (MSE). Accordingly, Eqs. (6) to (11) present the formula of R, R^2, SAE, MAE, AARD, and MSE, correspondingly[71].

$$R = \sqrt{1 - \left\{ \sum_{i=1}^{NoD} \left(DV^{\exp} - DV^{cal}\right)_i^2 \Big/ \sum_{i=1}^{NoD} \left(DV^{\exp} - \overline{DV^{\exp}}\right)_i^2 \right\}} \tag{6}$$

$$R^2 = 1 - \left\{ \sum_{i=1}^{NoD} \left(DV^{\exp} - DV^{cal}\right)_i^2 \Big/ \sum_{i=1}^{NoD} \left(DV^{\exp} - \overline{DV^{\exp}}\right)_i^2 \right\} \tag{7}$$

$$SAE = \sum_{i=1}^{NoD} \left| DV^{\exp} - DV^{cal} \right|_i \tag{8}$$

$$MAE = (1/NoD) \times \sum_{i=1}^{NoD} \left| DV^{\exp} - DV^{cal} \right|_i \tag{9}$$

$$AARD = (100/NoD) \times \sum_{i=1}^{NoD} \left(\left| DV^{\exp} - DV^{cal} \right| / DV^{\exp} \right)_i \tag{10}$$

$$MSE = (1/NoD) \times \sum_{i=1}^{NoD} \left(DV^{\exp} - DV^{cal} \right)_i^2 \tag{11}$$

The above equations need experimental ($DV^{\exp}$) and calculated (DV^{cal}) dependent variables as well as the average value of the $DV^{\exp}$. Equation (12) calculates this average value, i.e., $\overline{DV^{\exp}}$.

$$\overline{DV^{\exp}} = \sum_{i=1}^{NoD} \left(DV^{\exp}\right)_i / NoD \tag{12}$$

Results and discussions

This section introduces the results of relevancy analysis by MLR, MLP-ANN development, and statistical and graphical investigations of the proposed model.

Relevancy analysis by the multiple linear regression. Before constructing the MLP-ANN to estimate the CO_2 permeability in PMP/nanoparticle membranes, the relevancy between dependent and dependent variables must be explored. The MLR is a well-known method in this field[72]. Equation (13) is a simple MLR model that correlates the normalized CO_2 permeability (Y^{cal}) to the normalized values of the independent variables based on 112 experimental datasets.

$$Y^{cal} = 0.13745 + 0.05607\,X_1 + 0.48741\,X_2 + 0.21084\,X_3 \tag{13}$$

The positive sign of the X_1, X_2, and X_3 coefficients suggests the direct dependency of CO_2 permeability on the involved independent variables. Also, the coefficient magnitude shows the strength of the relationship between the dependent and independent variables. As Fig. 3 illustrates the CO_2 permeability in PMP/nanoparticle membranes has the strongest dependency on the nanoparticle dose and the weakest dependency on the additive type.

The observed AARD = 88.24%, R^2 = 0.40145, and SAE = 7634.84 barrer between experimental CO_2 permeabilities and MLR predictions show that the considered problem is mainly governed by a nonlinear model.

The accuracy of indices is calculated after de-normalizing the MLR prediction for the normalized CO_2 permeability using Eq. (14).

$$DV^{cal} = Y^{cal} \times \left(DV^{\max} - DV^{\min}\right) + DV^{\min} \begin{cases} DV^{\min} = 18.01 \\ DV^{\max} = 570.90 \end{cases} \tag{14}$$

Nonlinear modeling by the MLP-ANN. The general topology of the MLP-ANN to relate the CO_2 permeability in PMP/nanoparticle MMMs has been shown in Fig. 4.

This stage constructs 90 MLP-ANN approaches with different numbers of hidden neurons. Indeed, these MLP-ANN models may have one to nine neurons in their hidden layers. In addition, the MLP-ANN with a specific number of hidden neurons is trained and tested 10 different times.

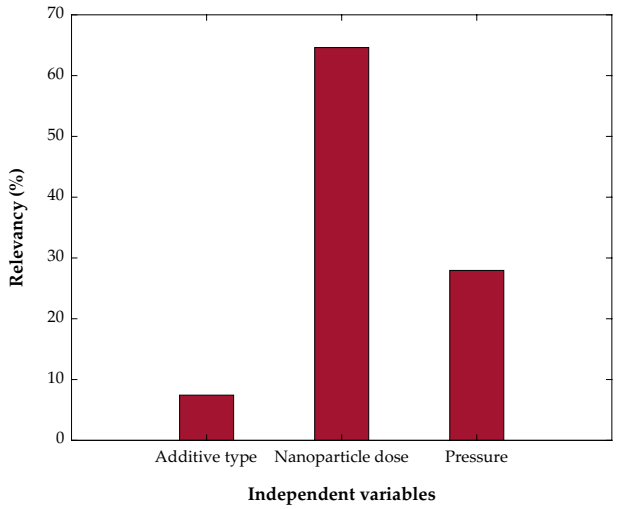

Figure 3. Relevancy between CO_2 permeability in MMMs and additive type, nanoparticle dose, and pressure.

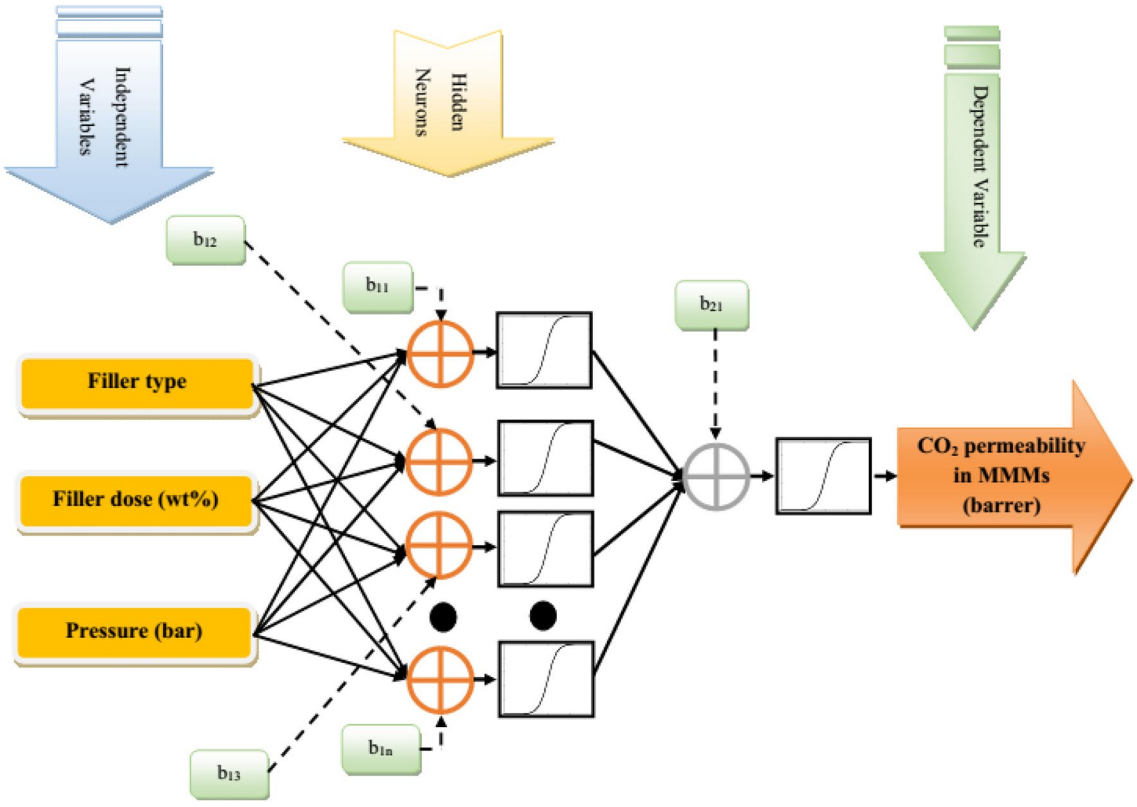

Figure 4. The MLP-ANN structure to simulate CO_2 permeability in PMP/nanoparticle MMMs.

Figure 5 shows the results of ranking the 90 constructed MLP-ANN models. Generally, the MLP-ANN accuracy increases (rank decreases) by increasing the number of hidden neurons. This observation is related to the increasing MLP-ANN size as well as the number of their weights and biases. The figure indicates that the second-developed MLP-ANN with eight hidden neurons (rank = 1) is the best model for estimating the CO_2 permeability in PMP/nanoparticle MMMs. In addition, the 9th-built MLP-ANN with only one hidden layer is the lowest accurate model (rank = 90) for the considered task.

The best MLP-ANN is applied to accomplish all subsequent analyses and the remaining 89 models are ignored.

Figure 6 presents the general shape of the MLP-ANN approach constructed to estimate the CO_2 permeability in MMMs. It can be seen that the MLP-ANN has only one hidden layer with eight neurons, i.e., 3-8-1 topology. The hyperbolic tangent sigmoid and logarithmic sigmoid transfer functions can also be seen in the hidden

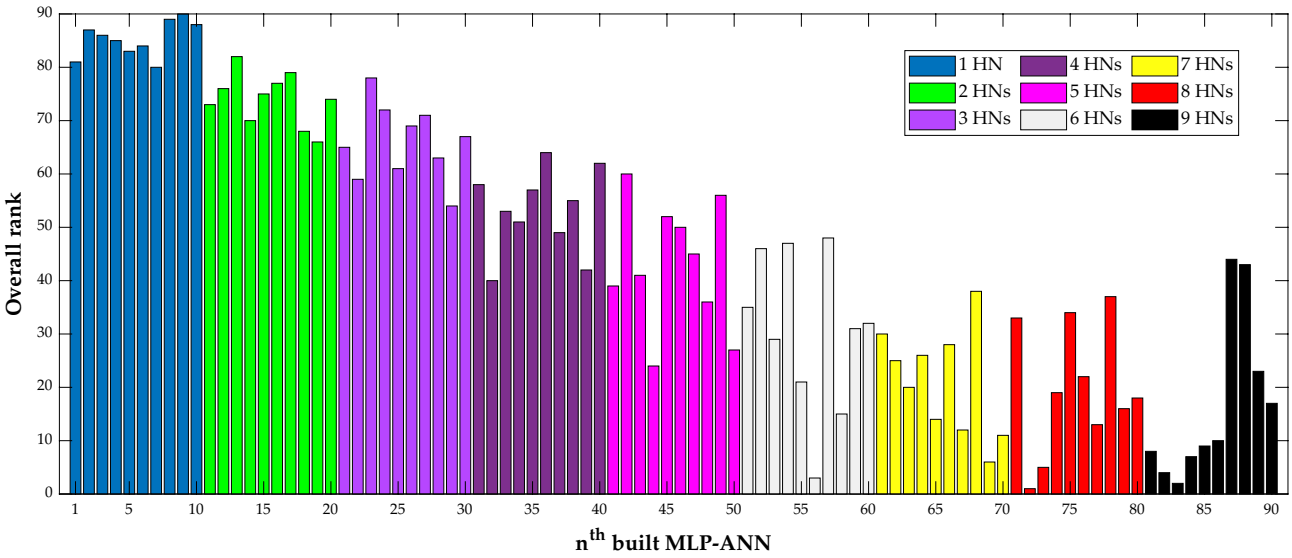

Figure 5. Overall ranking of the 90 constructed MLP-ANNs with 1–9 hidden neurons (10 models per each hidden neuron).

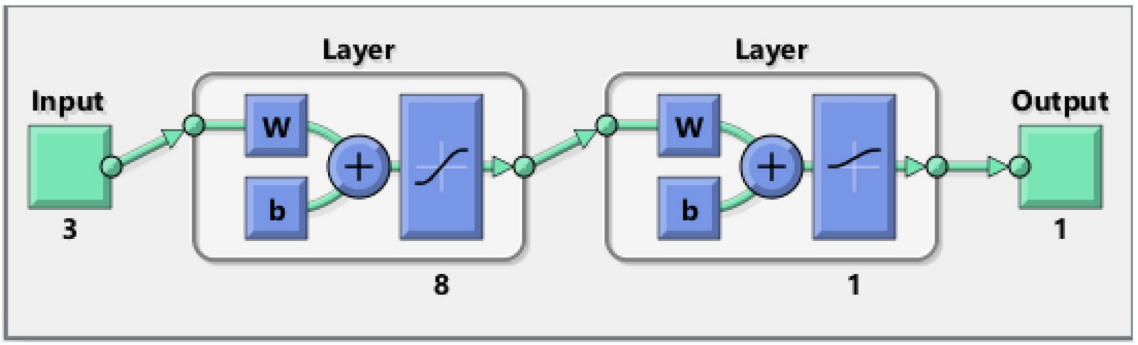

Figure 6. Topology of the best MLP-ANN[73] for predicting CO_2 permeability in PMP/nanoparticle membranes.

and output layers. It should be noted that the modeling phase of the CO_2 permeability in both PMP and PMP/nanoparticle membranes is done in the MATLAB environment (Version: 2019a)[73].

Table 3 reports the achieved accuracy of the proposed MLP-ANN in the training and testing stages. This table also shows the accuracy of the built MLP-ANN model for predicting the CO_2 permeability of the overall datasets. Five statistical criteria (i.e., R, MAE, AARD, MSE, and SAE) have been used in this regard. All these accuracies are acceptable enough from the modeling point of view.

Performance checking. The cross-plot which graphically inspects the linear correlation between experimental and predicted values of a dependent variable is a practical method to evaluate the reliability of data-driven models. Figure 7a–c illustrate the linear correlation between experimental CO_2 permeabilities and their associated calculated values by the MLP-ANN approach. Since both training and testing datasets are mainly located around the diagonal lines, the MLP-ANN reliability is approved by the visual inspection. Moreover, the closeness of the correlation coefficients of the training, testing, and all datasets to $R \sim 1$ (i.e., 0.99658, 0.98433, and 0.99477) is another indication of the MLP-ANN model.

The actual and predicted CO_2 permeabilities in the pure PMP membranes and PMP/nanoparticles MMMs in the training, as well as testing stages are depicted in Fig. 8. This analysis justifies the outstanding performance of

Data group	R	MAE	AARD	MSE	SAE
Training group	0.99658	5.28	5.20%	100.54	501.84
Testing group	0.98433	15.76	6.88%	444.52	267.84
Overall data	0.99477	6.87	5.46%	152.75	769.68

Table 3. Accuracy of the best MLP-ANN for estimating the CO_2 permeability in MMMs.

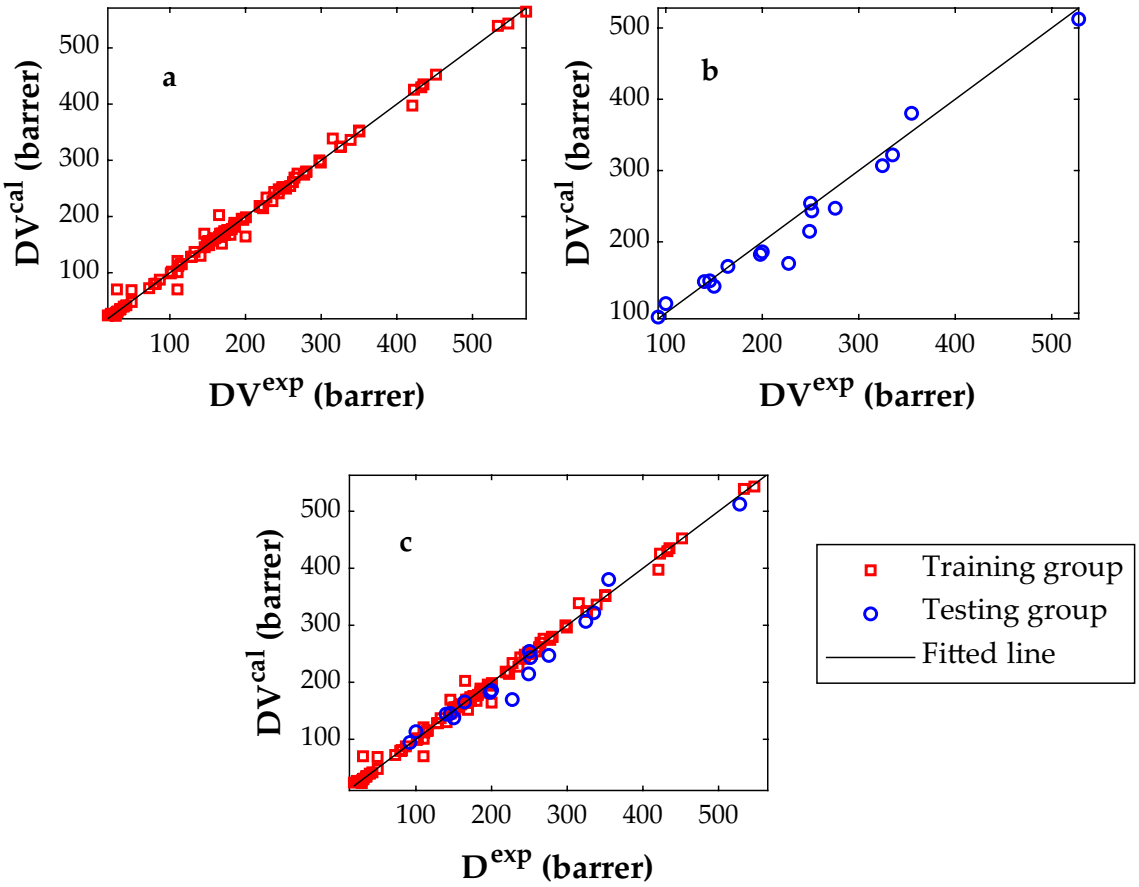

Figure 7. Linear correlations between experimental and calculated CO_2 permeability in MMMs; training (**a**), testing (**b**), and overall database (**c**).

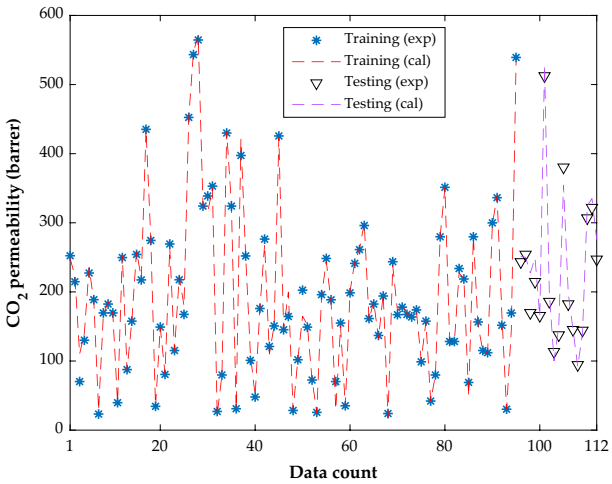

Figure 8. Compatibility between experimen6tal and calculated CO_2 permeability in MMMs.

the MLP-ANN to model both training and testing datasets. In addition, the MLP-ANN accuracy for predicting the training (MAE = 5.28, AARD = 5.20%, MSE = 100.54, and SAE = 501.84) and testing group (MAE = 15.76, AARD = 6.88%, MSE = 444.52, and SAE = 267.84) is approved by the statistical investigation. In addition, the overall values of the MAE, AARD, MSE, and SAE are 6.87, 5.46%, 152.75, and 769.68, correspondingly.

Trend analysis. Figure 9 explains the effect of alumina concentration on CO_2 permeability in the PMP/Al_2O_3 membrane from the modeling and experimental point of view. The outstanding agreement between actual and estimated CO_2 permeabilities in the PMP/Al_2O_3 MMMs can be easily found in this figure. The MLP-ANN

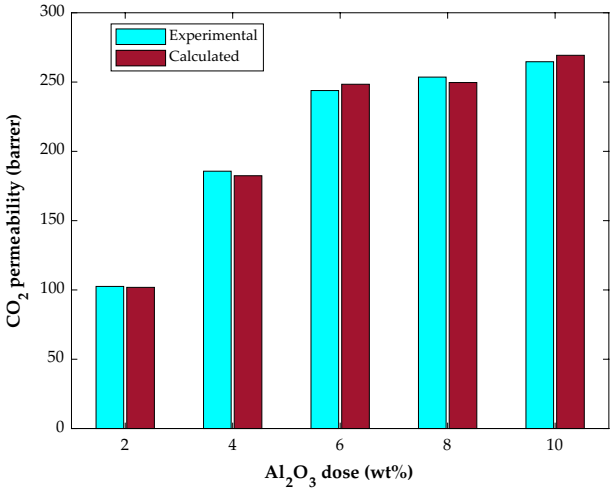

Figure 9. The effect of additive dose on the CO_2 permeability in PMP/Al_2O_3 membranes (pressure = 10 bar).

also accurately learns the increasing effect of the filler dose on CO_2 separation by the membrane-based process. Increasing the CO_2 permeability in membranes by increasing the filler dose was also previously forecasted by the MLR relevancy investigation.

The literature has related this permeability improvement to the alumina-polymer interactions and pore volume increment due to the Al_2O_3 presence within the polymer chain[61].

The effect of working pressure on CO_2 separation by the PMP/ZnO membranes with five nanoparticle concentration levels (2.5, 5, 8, 10, and 15 wt%) has been presented in Fig. 10. This figure displays both laboratory-measured CO_2 permeabilities and their related MLP-ANN predictions. An excellent agreement between the experimental and modeling permeability-pressure profiles is easily observable through this investigation. The MLP-ANN also correctly identifies the pressure as well as the filler effect on CO_2 permeability in PMP/ZnO mixed matrix membranes.

As expected, the CO_2 permeability in the mixed matrix membranes rises by increasing the working pressure. This observation is in a direct relationship with the driving force improvement due to the pressure enhancement.

The effect of filler type (ZnO, Al_2O_3, TiO_2, and TiO_2-NT) on the CO_2 separation ability of PMP-based membranes in the same working pressure is illustrated in Fig. 11. It can be seen that different fillers represent various roles in CO_2-MMM interaction. Indeed, the PMP/TiO_2 and PMP-TiO_2-NT provide the CO_2 molecule with minimum and maximum permeabilities within the membrane structure. The literature justified the higher CO_2 permeability in PMP-TiO_2-NT to the free volume expansion and porosity increase due to the functionalized nanoparticle presence in the membrane body[60].

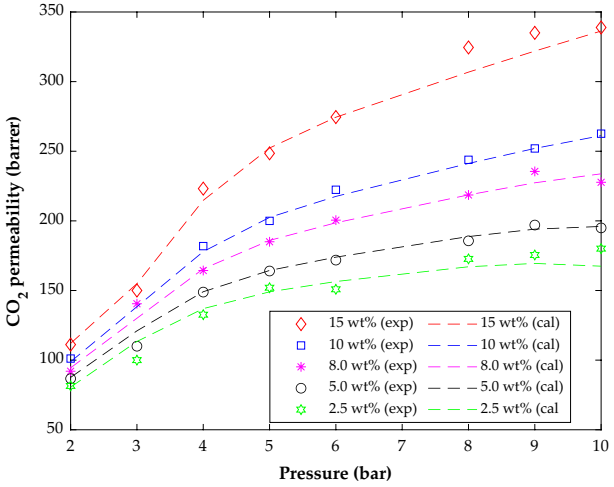

Figure 10. The effect of pressure on the CO_2 permeability in PMP/ZnO membranes with different additive dosages.

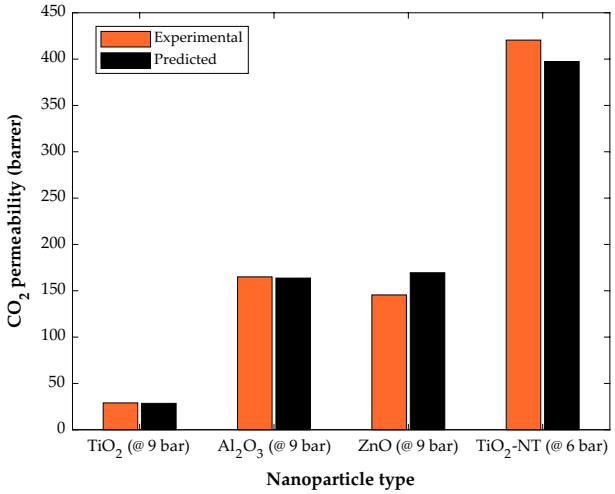

Figure 11. The effect of additive type on the CO_2 permeability in PMP/nanoparticle membranes.

Conclusions

This study uses a two-step methodology, i.e., multiple linear regression and multilayer perceptron artificial neural networks to simulate carbon dioxide permeability in mixed matrix membranes. The carbon dioxide permeability in pure poly(4-methyl-1-pentene) and PMP/nanoparticle membranes (i.e., PMP/ZnO, PMP/Al_2O_3, PMP/TiO_2, and PMP/TiO_2-NT) has been studied based on 112 experimental datasets collected from the literature. The multiple linear regression method applies to anticipate the dependency of the carbon dioxide permeability on the membrane composition (additive type and dose) and pressure. This method shows that the carbon dioxide permeability is directly related to all independent variables and it has the strongest correlation with the nanoparticle dose in membrane structure. The MLP-ANN is then utilized to construct a non-linear approach to estimate the carbon dioxide permeability as a function of additive type, nanoparticle dose, and pressure. This MLP-ANN with the 3-8-1 topology predicted 112 experimental carbon dioxide permeabilities in the involved MMMs with excellent accuracy (i.e., R = 0.99477, MAE = 6.87, AARD = 5.46%, MSE = 152.75, and SAE = 769.68). The modeling results clarify that the PMP/TiO_2-NT has a better carbon dioxide separation than the PMP/ZnO, PMP/Al_2O_3, and PMP/TiO_2 mixed matrix membranes. Finally, the obtained results in this work demonstrated the excellent potential of the ANN for estimating the separation factors of mixed matrix membranes for carbon capture and sequestration applications.

Data availability

All the literature datasets analyzed in this study are available at a reasonable request from the corresponding author (S.A. Abdollahi).

Received: 22 March 2023; Accepted: 29 May 2023
Published online: 31 May 2023

References

1. Wennersten, R., Sun, Q. & Li, H. The future potential for Carbon Capture and Storage in climate change mitigation—An overview from perspectives of technology, economy and risk. *J. Clean. Prod.* **103**, 724–736 (2015).
2. Du, L., Lu, T. & Li, B. CO_2 capture and sequestration in porous media with SiO_2 aerogel nanoparticle-stabilized foams. *Fuel* **324**, 124661 (2022).
3. Karimi, M. *et al.* CO_2 capture in chemically and thermally modified activated carbons using breakthrough measurements: experimental and modeling study. *Ind. Eng. Chem. Res.* **57**, 11154–11166 (2018).
4. Karimi, M. *et al.* MIL-160 (Al) as a candidate for biogas upgrading and CO_2 capture by adsorption processes. *Ind. Eng. Chem. Res.* **62**, 5216–5229 (2023).
5. Change, I. C. Impacts, Adaptation, and Vulnerability. Working Group II Contribution to the IPCC Sixth Assessment Report of the Intergovernmental Panel on Climate Change; Pötner, H. *O., Roberts, DC, Tignor, M., Poloczanska, ES, Mintenbeck, K., Ale, A., Eds* (2022).
6. Lu, J., Chen, H. & Cai, X. From global to national scenarios: Exploring carbon emissions to 2050. *Energy Strateg. Rev.* **41**, 100860 (2022).
7. Yu, C.-H., Huang, C.-H. & Tan, C.-S. A review of CO_2 capture by absorption and adsorption. *Aerosol Air Qual. Res.* **12**, 745–769 (2012).
8. Karimi, M., Shirzad, M., Silva, J. A. C. & Rodrigues, A. E. Carbon dioxide separation and capture by adsorption: A review. *Environ. Chem. Lett.* https://doi.org/10.1007/s10311-023-01589-z (2023).
9. Xi, M. *et al.* Predicted a honeycomb metallic BiC and a direct semiconducting Bi_2C monolayer as excellent CO_2 adsorbents. *Chin. Chem. Lett.* **33**, 2595–2599 (2022).
10. Xu, G. *et al.* A novel CO_2 cryogenic liquefaction and separation system. *Energy* **42**, 522–529 (2012).
11. Rafiq, S. *et al.* Surface tuning of silica by deep eutectic solvent to synthesize biomass derived based membranes for gas separation to enhance the circular bioeconomy. *Fuel* **310**, 122355 (2022).
12. Zhao, B. *et al.* Study on corrosion in CO_2 chemical absorption process using amine solution. *Energy Procedia* **4**, 93–100 (2011).

13. Lamy-Mendes, A. *et al.* Amine modification of silica aerogels/xerogels for removal of relevant environmental pollutants. *Molecules* **24**, 3701 (2019).
14. Lu, W., Bosch, M., Yuan, D. & Zhou, H. Cost-effective synthesis of amine-tethered porous materials for carbon capture. *Chemsuschem* **8**, 433–438 (2015).
15. Song, C. *et al.* Reducing the energy consumption of membrane-cryogenic hybrid CO_2 capture by process optimization. *Energy* **124**, 29–39 (2017).
16. Karimi, M., Shirzad, M., Silva, J. A. C. & Rodrigues, A. E. Biomass/biochar carbon materials for CO_2 capture and sequestration by cyclic adsorption processes: A review and prospects for future directions. *J. CO2 Util.* **57**, 101890 (2022).
17. Siegelman, R. L., Milner, P. J., Kim, E. J., Weston, S. C. & Long, J. R. Challenges and opportunities for adsorption-based CO_2 capture from natural gas combined cycle emissions. *Energy Environ. Sci.* **12**, 2161–2173 (2019).
18. Gasós, A., Becattini, V., Brunetti, A., Barbieri, G. & Mazzotti, M. Process performance maps for membrane-based CO_2 separation using artificial neural networks. *Int. J. Greenh. Gas Control* **122**, 103812 (2023).
19. Lin, X. *et al.* Membrane inlet mass spectrometry method (REOX/MIMS) to measure 15N-nitrate in isotope-enrichment experiments. *Ecol. Indic.* **126**, 107639 (2021).
20. Miltner, M., Makaruk, A. & Harasek, M. Review on available biogas upgrading technologies and innovations towards advanced solutions. *J. Clean. Prod.* **161**, 1329–1337 (2017).
21. Uddin, M. W. & Hägg, M.-B. Effect of monoethylene glycol and triethylene glycol contamination on CO_2/CH_4 separation of a facilitated transport membrane for natural gas sweetening. *J. Memb. Sci.* **423**, 150–158 (2012).
22. Zhao, C., Xi, M., Huo, J., He, C. & Fu, L. Computational design of BC3N2 based single atom catalyst for dramatic activation of inert CO_2 and CH_4 gasses into CH_3COOH with ultralow CH_4 dissociation barrier. *Chin. Chem. Lett.* **34**, 107213 (2023).
23. Ahmad, A. *et al.* Recent trends and challenges with the synthesis of membranes: Industrial opportunities towards environmental remediation. *Chemosphere* **306**, 135634. https://doi.org/10.1016/j.chemosphere.2022.135634 (2022).
24. Yeo, Z. Y., Chai, S.-P., Zhu, P. W. & Mohamed, A. R. An overview: synthesis of thin films/membranes of metal organic frameworks and its gas separation performances. *RSC Adv.* **4**, 54322–54334 (2014).
25. Dong, G., Li, H. & Chen, V. Challenges and opportunities for mixed-matrix membranes for gas separation. *J. Mater. Chem. A* **1**, 4610–4630 (2013).
26. Jee, K. Y. & Lee, Y. T. Preparation and characterization of siloxane composite membranes for n-butanol concentration from ABE solution by pervaporation. *J. Memb. Sci.* **456**, 1–10 (2014).
27. Budd, P. M. & McKeown, N. B. Highly permeable polymers for gas separation membranes. *Polym. Chem.* **1**, 63–68 (2010).
28. Chen, X. Y., Hoang, V.-T., Rodrigue, D. & Kaliaguine, S. Optimization of continuous phase in amino-functionalized metal–organic framework (MIL-53) based co-polyimide mixed matrix membranes for CO_2/CH_4 separation. *RSC Adv.* **3**, 24266–24279 (2013).
29. Pereira, V. R. *et al.* Preparation and performance studies of polysulfone-sulfated nano-titania (S-TiO_2) nanofiltration membranes for dye removal. *RSC Adv.* **5**, 53874–53885 (2015).
30. Bhadra, P. *et al.* Selective transportation of charged ZnO nanoparticles and microorganism dialysis through silicon nanoporous membranes. *J. Memb. Sci.* **503**, 16–24 (2016).
31. Suleman, M. S., Lau, K. K. & Yeong, Y. F. Plasticization and swelling in polymeric membranes in CO_2 removal from natural gas. *Chem. Eng. Technol.* **39**, 1604–1616 (2016).
32. Clarizia, G., Algieri, C. & Drioli, E. Filler-polymer combination: A route to modify gas transport properties of a polymeric membrane. *Polymer (Guildf).* **45**, 5671–5681 (2004).
33. Ali, A., Mubashir, M., Abdulrahman, A. & Phelan, P. E. Ultra-permeable intercalated metal-induced microporous polymer nanodots rooted smart membrane for environmental remediation. *Chemosphere* **306**, 135482 (2022).
34. Yang, G. C. C. & Tsai, C.-M. Effects of starch addition on characteristics of tubular porous ceramic membrane substrates. *Desalination* **233**, 129–136 (2008).
35. Maguire-Boyle, S. J. *et al.* Superhydrophilic functionalization of microfiltration ceramic membranes enables separation of hydrocarbons from frac and produced water. *Sci. Rep.* **7**, 12267 (2017).
36. Lee, J.-Y., Tang, C. Y. & Huo, F. Fabrication of porous matrix membrane (PMM) using metal-organic framework as green template for water treatment. *Sci. Rep.* **4**, 1–5 (2014).
37. Ismail, A. F., Goh, P. S., Sanip, S. M. & Aziz, M. Transport and separation properties of carbon nanotube-mixed matrix membrane. *Sep. Purif. Technol.* **70**, 12–26 (2009).
38. Talukder, M. E. *et al.* Ag nanoparticles immobilized sulfonated polyethersulfone/polyethersulfone electrospun nanofiber membrane for the removal of heavy metals. *Sci. Rep.* **12**, 5814 (2022).
39. Xue, B. *et al.* An AuNPs/mesoporous NiO/nickel foam nanocomposite as a miniaturized electrode for heavy metal detection in groundwater. *Engineering*. https://doi.org/10.1016/j.eng.2022.06.005 (2022).
40. Wang, Z. *et al.* Enhanced denitrification performance of Alcaligenes sp TB by Pd stimulating to produce membrane adaptation mechanism coupled with nanoscale zero-valent iron. *Sci. Total Environ.* **708**, 135063 (2020).
41. Ahn, J., Chung, W.-J., Pinnau, I. & Guiver, M. D. Polysulfone/silica nanoparticle mixed-matrix membranes for gas separation. *J. Memb. Sci.* **314**, 123–133 (2008).
42. Pechar, T. W., Tsapatsis, M., Marand, E. & Davis, R. Preparation and characterization of a glassy fluorinated polyimide zeolite-mixed matrix membrane. *Desalination* **146**, 3–9 (2002).
43. Ismail, A. F., Rahim, R. A. & Rahman, W. Characterization of polyethersulfone/Matrimid® 5218 miscible blend mixed matrix membranes for O_2/N_2 gas separation. *Sep. Purif. Technol.* **63**, 200–206 (2008).
44. Tang, F., Niu, B., Zong, G., Zhao, X. & Xu, N. Periodic event-triggered adaptive tracking control design for nonlinear discrete-time systems via reinforcement learning. *Neural Netw.* **154**, 43–55 (2022).
45. Si, Z., Yang, M., Yu, Y. & Ding, T. Photovoltaic power forecast based on satellite images considering effects of solar position. *Appl. Energy* **302**, 117514 (2021).
46. Guedes, I. A. *et al.* New machine learning and physics-based scoring functions for drug discovery. *Sci. Rep.* **11**, 1–19 (2021).
47. Cheng, F., Liang, H., Niu, B., Zhao, N. & Zhao, X. Adaptive neural self-triggered bipartite secure control for nonlinear MASs subject to DoS attacks. *Inf. Sci. (Ny)* **631**, 256–270 (2023).
48. Bansal, M., Goyal, A. & Choudhary, A. A comparative analysis of K-Nearest Neighbour, Genetic, Support Vector Machine, Decision Tree, and Long Short Term Memory algorithms in machine learning. *Decis. Anal. J.* **3**, 100071 (2022).
49. Li, Z., Wang, J., Huang, J. & Ding, M. Development and research of triangle-filter convolution neural network for fuel reloading optimization of block-type HTGRs. *Appl. Soft Comput.* https://doi.org/10.1016/j.asoc.2023.110126 (2023).
50. Dragoi, E.-N. & Vasseghian, Y. Modeling of mass transfer in vacuum membrane distillation process for radioactive wastewater treatment using artificial neural networks. *Toxin Rev.* **40**, 1526–1535 (2021).
51. Rezakazemi, M., Dashti, A., Asghari, M. & Shirazian, S. H_2-selective mixed matrix membranes modeling using ANFIS, PSO-ANFIS, GA-ANFIS. *Int. J. Hydrogen Energy* **42**, 15211–15225 (2017).
52. Karimi, M., Hosin Alibak, A., Seyed Alizadeh, S. M., Sharif, M. & Vaferi, B. Intelligent modeling for considering the effect of biosource type and appearance shape on the biomass heat capacity. *Meas. J. Int. Meas. Confed.* **189**, 110529 (2022).
53. Chamani, H. *et al.* CFD-based genetic programming model for liquid entry pressure estimation of hydrophobic membranes. *Desalination* **476**, 114231 (2020).

54. Rezakazemi, M., Mosavi, A. & Shirazian, S. ANFIS pattern for molecular membranes separation optimization. *J. Mol. Liq.* **274**, 470–476 (2019).
55. Vural, Y., Ingham, D. B. & Pourkashanian, M. Performance prediction of a proton exchange membrane fuel cell using the ANFIS model. *Int. J. Hydrogen Energy* **34**, 9181–9187 (2009).
56. Zhao, Z. *et al.* Prediction of interfacial interactions related with membrane fouling in a membrane bioreactor based on radial basis function artificial neural network (ANN). *Bioresour. Technol.* **282**, 262–268 (2019).
57. Kazemian, H. B., White, K. & Palmer-Brown, D. Applications of evolutionary SVM to prediction of membrane alpha-helices. *Expert Syst. Appl.* **40**, 3412–3420 (2013).
58. Saeedi Dehaghani, A. H. & Pirouzfar, V. Preparation of high-performance membranes derived from poly (4-methyl-1-pentene)/zinc oxide particles. *Chem. Eng. Technol.* **40**, 1693–1701 (2017).
59. Alihosseini, A., Zergani, D. & Saeedi Dehaghani, A. H. Optimization of parameters affecting separation of gas mixture of O_2, N_2, CO_2 and CH_4 by PMP membrane modified with TiO_2, ZnO and Al_2O_3 nanoparticles. *Polyolefins J.* **7**, 13–24 (2019).
60. Saeedi Dehaghani, A. H., Pirouzfar, V. & Alihosseini, A. Novel nanocomposite membranes-derived poly (4-methyl-1-pentene)/functionalized titanium dioxide to improve the gases transport properties and separation performance. *Polym. Bull.* **77**, 6467–6489 (2020).
61. Nematollahi, M. H., Dehaghani, A. H. S., Pirouzfar, V. & Akhondi, E. Mixed matrix membranes comprising PMP polymer with dispersed alumina nanoparticle fillers to separate CO_2/N_2. *Macromol. Res.* **24**, 782–792 (2016).
62. Guidotti, R. *et al.* A survey of methods for explaining black box models. *ACM Comput. Surv.* **51**, 1–42 (2018).
63. Leperi, K. T., Yancy-Caballero, D., Snurr, R. Q. & You, F. 110th anniversary: surrogate models based on artificial neural networks to simulate and optimize pressure swing adsorption cycles for CO_2 capture. *Ind. Eng. Chem. Res.* **58**, 18241–18252 (2019).
64. Waqas, S. *et al.* SVM and ANN modelling approach for the optimization of membrane permeability of a membrane rotating biological contactor for wastewater treatment. *Membranes (Basel).* **12**, 821 (2022).
65. Ke, K.-C. & Huang, M.-S. Quality prediction for injection molding by using a multilayer perceptron neural network. *Polymers (Basel).* **12**, 1812 (2020).
66. Pu, L., Li, Y., Gao, P., Zhang, H. & Hu, J. A photosynthetic rate prediction model using improved RBF neural network. *Sci. Rep.* **12**, 9563 (2022).
67. Ren, K., Jiao, Z., Wu, X.-L. & Han, H.-G. Multivariable identification of membrane fouling based on compacted cascade neural network. *Chin. J. Chem. Eng.* **53**, 37–45 (2023).
68. Fulcher, J. A. A comparative review of commercial ANN simulators. *Comput. Stand. interfaces* **16**, 241–251 (1994).
69. Curteanu, S. & Cartwright, H. Neural networks applied in chemistry. I. Determination of the optimal topology of multilayer perceptron neural networks. *J. Chemom.* **25**, 527–549 (2011).
70. Díez, J.-L., Masip-Moret, V., Santafé-Moros, A. & Gozálvez-Zafrilla, J. M. Comparison of artificial intelligence control strategies for a peristaltically pumped low-pressure driven membrane process. *Membranes (Basel).* **12**, 883 (2022).
71. Abdollahzadeh, M. *et al.* Estimating the density of deep eutectic solvents applying supervised machine learning techniques. *Sci. Rep.* **12**, 1–16 (2022).
72. Wang, J. *et al.* Prediction of CO_2 solubility in deep eutectic solvents using random forest model based on COSMO-RS-derived descriptors. *Green Chem. Eng.* **2**, 431–440 (2021).
73. MATLAB and Artificial Neural Networks Toolbox (Release 2019a), The MathWorks, Inc., Natick, Massachusetts, United States. (2019).

Author contributions

S.A.A.: preparing the original draft, collecting the literature data, data curation, model construction, formal analysis. S.F.R.: preparing the original draft, relevancy analysis, conceptualization, final approval, supervision.

Competing interests

The authors declare no competing interests.

Additional information

Correspondence and requests for materials should be addressed to S.A.A.

Reprints and permissions information is available at www.nature.com/reprints.

Publisher's note Springer Nature remains neutral with regard to jurisdictional claims in published maps and institutional affiliations.